Hindawi
Journal of Nanomaterials
Volume 2021, Article ID 9076170, 13 pages
https://doi.org/10.1155/2021/9076170

Research Article

Effect of Coupling Agent on Softwood Kraft Nanocellulose Fibril-Reinforced Polylactic Acid Biocomposite

Usman Saeed, Sami Ullah Rathur, Hamad AlTuraif, and Hisham Bamufleh

Department of Chemical and Materials Engineering, Faculty of Engineering, King Abdulaziz University, Jeddah 21441, Saudi Arabia

Correspondence should be addressed to Usman Saeed; usman144de@yahoo.com

Received 12 August 2021; Revised 2 November 2021; Accepted 29 November 2021; Published 24 December 2021

Academic Editor: P. Davide Cozzoli

The nanocellulose fibril produced by using natural sources can be used in developing sustainable and green products. The useful features of nanocellulose fibril can include valuable physical properties, appropriate surface chemistry, low toxicity, and biocompatibility. The study presented shows the use of polylactic acid with five different percentages of nanocellulose fibril and the use of 3% maleic anhydride as a coupling agent. The maleic anhydride acts as coupling agent which improves the thermochemical and thermomechanical characteristics of the end product. The addition of 3% maleic anhydride as coupling agent with 10% nanocellulose fibril improved the impact strength up to 14.3%, elastic modulus up to 40.6%, and tensile strength up to 30.1%. Furthermore, the dynamic mechanical analysis result indicates that the inclusion of maleic anhydride improved the toughness by reducing the tan δ peak and increases the storage modulus. Finally, the scanning electron micrograph shows that the interfacial compatibility between nanocellulose fibril and polylactic acid matrix is improved with the addition of maleic anhydride.

1. Introduction

The growing environmental concerns of plastic waste and pollution have paved the way for use of naturally sourced sustainable polymers instead of synthetic polymer. In the sustainable product development, natural polymers such as poly(lactic acid) (PLA), (butylene succinate) (PBS), and poly(butylenesadipate-co-terephthalate) (PBSA) are shown to be the most useful alternative to synthetic polymers as they are biocompatible and biodegradable [1–3]. The biopolymer degrades when disposed and returns all natural constituents to the environment helping in decreasing the plastic waste. In the naturally sourced polymers, PLA is a promising candidate for developing green products in comparison to synthetic polymers such as polyethylene, polypropylene, and polyethylene terephthalate. Also, PLA offers suitable physical properties (specific gravity and shrink rate) and thermal processing ability [3]. The disadvantages of using PLA can include innate brittleness, inadequate thermal stability, and lower quality of crystallization which limits its use in mass manufacturing in fields such as biomedical, packaging, energy storage, and automotive [4].

The natural fibers can help in forming green composite due to their cost-effectiveness, biodegradability, renewability, and low density. The naturally sourced fibers such as flex and kenaf are used to develop green composite because of their suitable tensile strength (280 ± 15 MPa) and elastic modulus (40 ± 5 GPa). The natural fibers when compared to synthetic glass, aramid, and carbon fiber have some disadvantages such as lower tensile strength, lower processing temperature, higher linear coefficients of thermal expansion, and moisture susceptibility [5]. In the natural fiber, the plant-derived cellulose can be used as reinforcement at the nanolevels which includes nanocellulose fibril (NCF) and nanocrystalline cellulose (NCC) [6–9]. The nanocellulose fibril (NCF) when used with polymer composite has shown excellent ability to act as nanoreinforcement, and it is cost-effective with respect to manufacturing. Moreover, the advantages of using NCF as nanoreinforcement include low density, strength, high stiffness, and biodegradability [10, 12]. There are studies performed to address the problem of brittleness with PLA by blending it with elastomeric materials such as rubber, copolymerizing with other monomer, and by utilizing plasticizer [13–15].

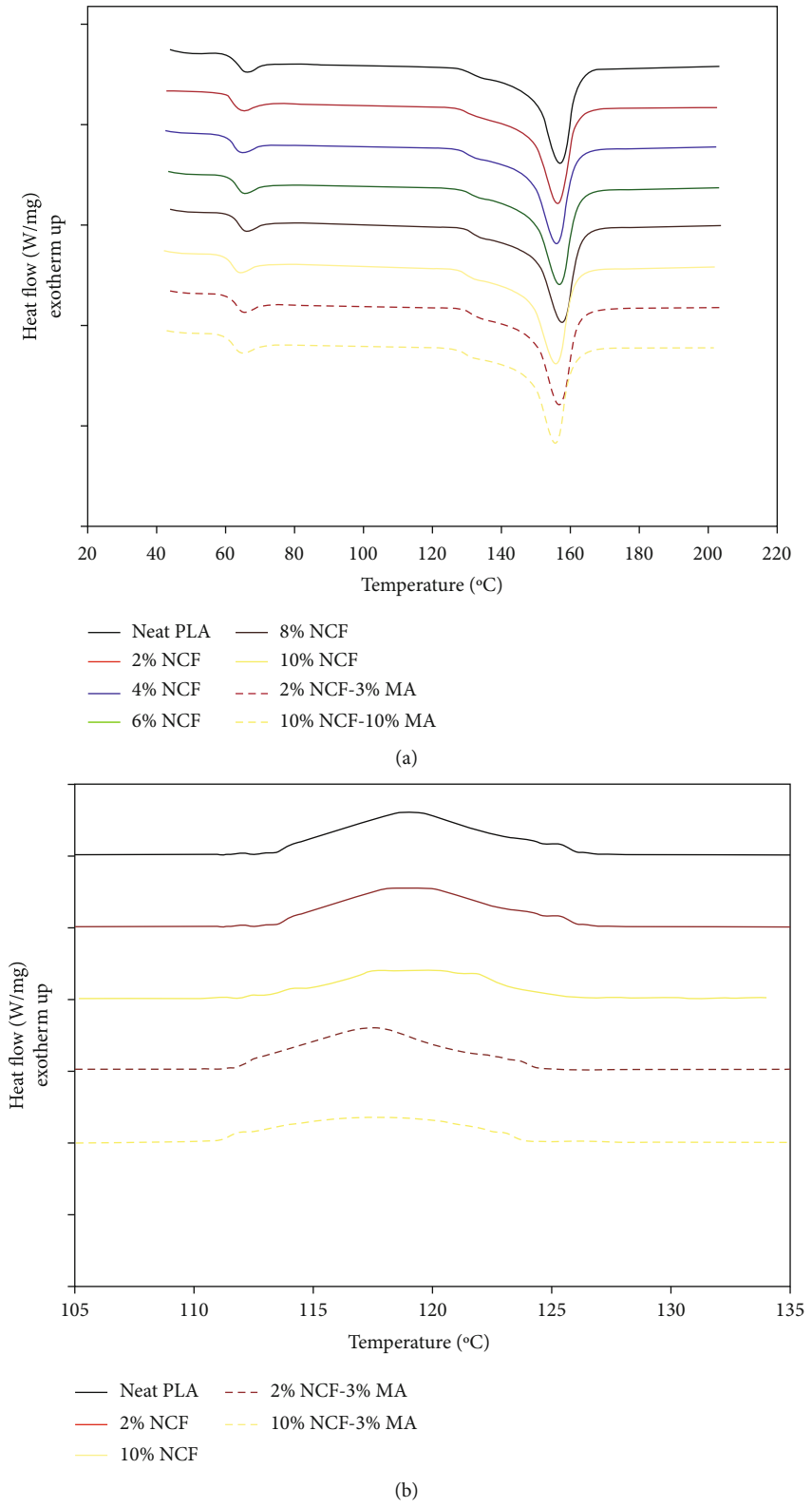

Figure 1: DSC thermogram of PLA-NCF-MA composite: (a) heating and (b) cooling.

However, the examiners described that even though there are substantial improvements in the toughness and ductility, the blends sacrificed their mechanical properties such as Young's modulus and strength. In one of the studies, PLA was reinforced with cellulose nanowhisker (CNW) and nanocellulose fibril (NCF) to improve the mechanical properties [16]. Additionally, there are issues related to uniform dispersion of nanocellulose fibril with

Table 1: Thermal properties of PLA-NCF-MA composites.

PLA-NCF-MA	T_g (°C)	T_m (°C)	T_c (°C)	ΔH_m (J/g)	X_c %
100/0/0	59.4	153.6	126.7	24.9	14.9
98/2/0	59.1	153.4	125.6	22.3	13.3
96/4/0	58.0	152.7	124.9	25.9	12.7
94/6/0	57.7	152.3	124.5	24.9	11.2
92/8/0	57.6	151.9	124.1	22.1	10.4
90/10/0	57.5	151.4	123.7	20.9	9.5
95/2/3	58.0	152.6	124.9	23.2	13.1
93/4/3	57.9	152.4	124.5	24.8	12.4
91/6/3	57.6	151.5	124.1	23.6	10.9
89/8/3	57.3	151.5	123.9	23.5	10.6
87/10/3	57.4	151.1	123.5	20.7	9.3

polar surfaces in the nonpolar polymers such as PLA [17–20]. The inhomogeneous distribution and low compatibility of NCF in polymer matrix resulted in end product with inadequate and unsuitable properties [21, 22]. The previous studies have shown that fiber-matrix interface is an important factor which predicts the characteristics of composite. To improve the interfacial adhesion between polymer and NCF, a study utilized a coupling agent and performed surface modification of nanocellulose fibrils (NCF) [23]. The studies also illustrated the use of functional elements found in PLA interact with nanocellulose by including maleic anhydride (MAH) as compatibilizer [24–26]. Carlson et al. showed the improvement in interfacial adhesion by mixing maleic anhydride in starch-reinforced PLA [27]. Also, Petersson and Oksman reported that the addition of microcrystalline cellulose reduces the barrier properties and mechanical strength of PLA biocomposite due to the less interaction between PLA matrix and cellulose [28]. Plackett indicated that by adding maleic anhydride interfacial adhesion can be improved between PLA and cellulose-based wood fiber [29]. To make biocomposite perform usefully, certain amount of adhesion was achieved between surface of the hydrophilic nanocellulose fibers and polymer matrix. The treatments such as grafting, isocyanate, dewaxing, and coupling agent were used to enhance the interfacial adhesion between natural fiber and polymer matrix [30]. The treatment of jute cellulose fiber with epoxy and silane showed improvement in mechanical properties such as elastic modulus, tensile strength, and hardness [31]. The coir fibers treated with enzyme influenced overall mechanical properties excluding flexural characteristic because of size of fibers [32]. The fibers were chemically treated by using benzoylation, acetylation, and acrylonitrile grafting. The structural stability and improved mechanical properties are the indicators showing the effects of chemical treatment of natural fiber in enhancement of interfacial adhesion [33]. The chemical treatment alternate hydrophilic nature of fiber helps in reducing the effect of moisture in the performance of composite [34]. The chemical treatments have the capability to alternate the physical and chemical properties of composites; therefore, it is necessary to examine the influence of maleated anhydride (MA) as coupling agent in nanocellulose fibril-reinforced PLA composite for improvement in interfacial adhesion.

In the research presented, the influence of 3% maleic anhydride (MA) as a coupling agent on variable NCF content (2 wt.%–10 wt.%)-reinforced polylactic acid (PLA) is being studied by evaluating chemistry, morphological, mechanical, and thermal properties. The characterization was performed by tensile test, differential scanning calorimetry (DSC), dynamic mechanical analysis (DMA), drop shape analyzer (DSA), and X-ray photo electron spectroscopy (XPS). Finally, fracture surface of the PLA-NCF-MA composites was analyzed by using scanning electron microscopy (SEM).

2. Materials and Methods

2.1. Preparation. NatureWorks, USA, provided the polylactic acid (PLA) 2003 D with melt flow index of 6 g/10 min. The University of Maine (Orono, USA) supplied water-based softwood kraft nanocellulose fibrils (NCF) having an average diameter of 30 nm-50 nm and approximate length of one micron. A stable dispersion with considerable transparency was being attained by dilution of NCF with Milli-Q water. The Milli-Q water helped in development of solution with NCF as 1.67 g/L. To produce the suspension, the solution was being stirred with the help of ultrasonic microtip for a time period of 10 min having amplitude of 25%. The Optima L-90K18 ultracentrifuge (Beckman Coulter, USA) was used to remove fibril aggregates by centrifuging at 10,000 rpm for 20 min. Finally, NCF was dried in spray dryer (BUCHI B290, Switzerland) before using it as reinforcement.

3% maleic anhydride (MA, Fusabond, MB100, DuPont, USA) was used as a coupling agent in PLA-NCF composite to improve adhesion between NCF and PLA. The NCF in five different concentrations ranging from 2% to 10% was mixed for 20 minutes with PLA and 3% maleic anhydride (MA) by using twin-screw extruder (Leistritz model ZSE27) with speed of 100 rpm at 180°C. The developed specimen was cooled in water, and a grinder was used for pelletizing. The drying of pellets was done for 24 h at 60°C. The hot compression moulding machine (Carver Press, Germany) was used to produce specimen for tensile test according to ASTM D638 type IV dimensions and 40 mm × 12mm × 5 mm dimensions for dynamic mechanical analysis. The hot compression moulding of pellets was performed for 2 minutes at 120°C with pressure of one ton. The developed PLA-NFC-MA composite specimens were cooled down to 25°C temperature under pressure for 24 h.

2.2. Characterization. The thermal behaviour of PLA-NCF-MA composite was examined by using the differential scanning calorimeter (DSC Netzsch 200 F3). The DSC thermogram was generated at 10°C min^{-1} from 20°C to 200°C for cooling and heating curves. The thermogram was used to examine the melting enthalpy, melting temperature, crystallization temperature, and degree of crystallinity (X_c %).

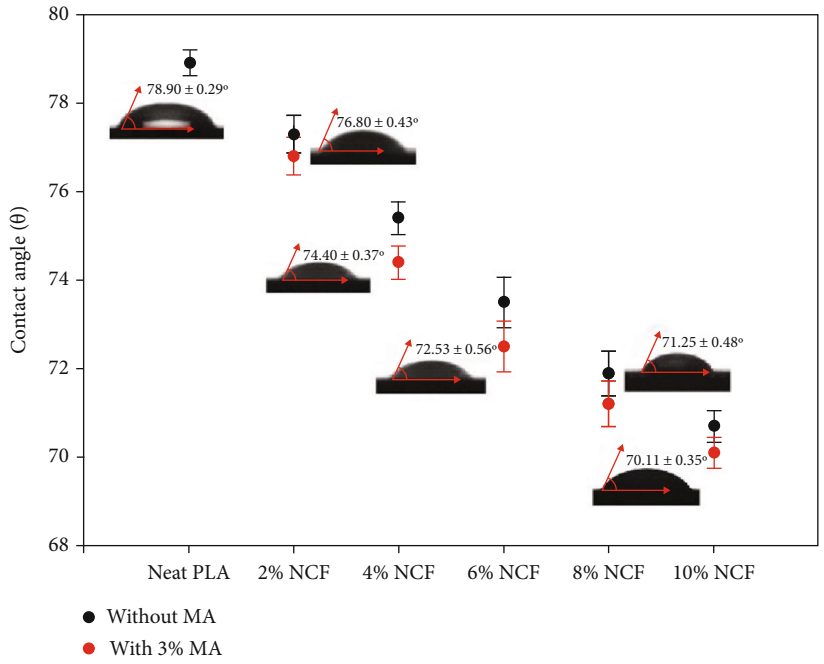

Figure 2: Contact angle of the PLA-NCF-MA composite (images of the drops present the values of NCF-PLA with 3% MA).

Equation (1) was used to evaluate the crystallinity (X_c %) of PLA-NCF-MA composite

$$X_c\% = \frac{\Delta H_m}{w \times \Delta H_m^o}, \quad (1)$$

where ΔH_m^o is melting enthalpy of 100% crystalline PLA (93.7 J/g), ΔH_m is the melting enthalpy, and w is the PLA weight fraction in PLA-NCF-MA composite.

The contact angle θ was characterized using a sessile drop of water on the surface of PLA-NCF-MA composite by employing drop shape analyzer (DSA 100, KRUSS, Germany). The water drop image on the surface of composites was taken to determine the contact angle in order to analyze the wetting. Three measurements of each composite specimen were evaluated to find the value of final contact angle.

The tensile testing machine (3369 Instron, USA) with 50 kN load cell was used to characterize the mechanical properties of PLA-NCF-MA composite having ASTM D638 type IV geometry. The test was performed with crosshead speed of 5 mm/min at 25°C having 0.500 N preload.

The impact testing machine (JB W300J, Poland) was utilized to perform Charpy impact test. The ASTMD256 dimensions of the specimen were 10 mm × 10 mm × 55 mm having 2 mm notch size. During the impact test, the impact speed was 5.2 m/s, potential impact energy was 150 J, and raise angle was 150°.

The dynamic mechanical analysis (DMA, 242, Netzsch, USA) was used to characterize PLA-NCF-MA composites for loss factor (tan δ) and storage modulus G'. The DMA functions with dual cantilever approach having sample dimensions of 40 mm × 12 mm × 5 mm. The DMA test was performed having 2°C/min heating rate, 1 Hz frequency, and 0.1% strain rate. During the test, the temperature was maintained between 30°C and 120°C.

The X-ray photo electron spectrometer (XPS, SPECS GmbH, Germany) was used at the pressure 1×10^{-8} mbar to characterize the PLA-NCF-MA composite. The composite specimen surfaces were irradiated by an X-ray source of 150 W and 13.5 kV utilizing dual anode nonmonochromatic Mg-K_α. The PLA-NCF-MA composite specimen was positioned having 90° take-off angle facing the direction of photoelectrons and surface of specimen. The atomic % concentration, energy of binding (BE), and bond type (C1s and O1s) orbital data were obtained by using a hemispherical energy analyzer (PHOIBOS 150 MCD-9) which was functioning in fixed analyzer transmission (FAT) mode.

The fracture surface of PLA-NCF-MA platinum-coated specimen was analyzed by using an electron microscope (JEOL JSM-7600F, MA) having 10 kV accelerating voltage.

All PLA-NCF-MA composite specimens with different compositions were three times examined by employing characterization methods to verify the final outcomes.

3. Results and Discussion

The heating and cooling curves are presented in Figures 1(a) and 1(b) for PLA-NCF-MA composites. The presented figures indicate the melting behaviour and crystallization of the composite. Also, Table 1 presents the assessed values of crystallinity (X_c %), glass transition temperature (T_g), crystallization temperature (T_c), melting enthalpy (ΔH_m), and melting temperature (T_m) of neat PLA and PLA-NCF-MA. The heating thermogram shows that the neat PLA has melting temperature T_m of 153.6°C. Table 1 demonstrates that T_m decreases up to 151.4°C with the rising increments of

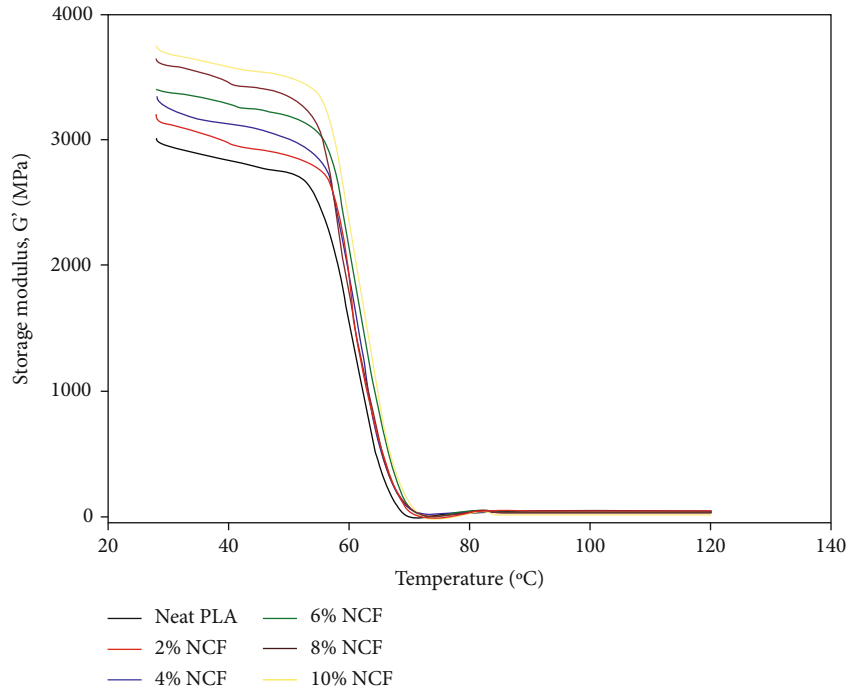

(a)

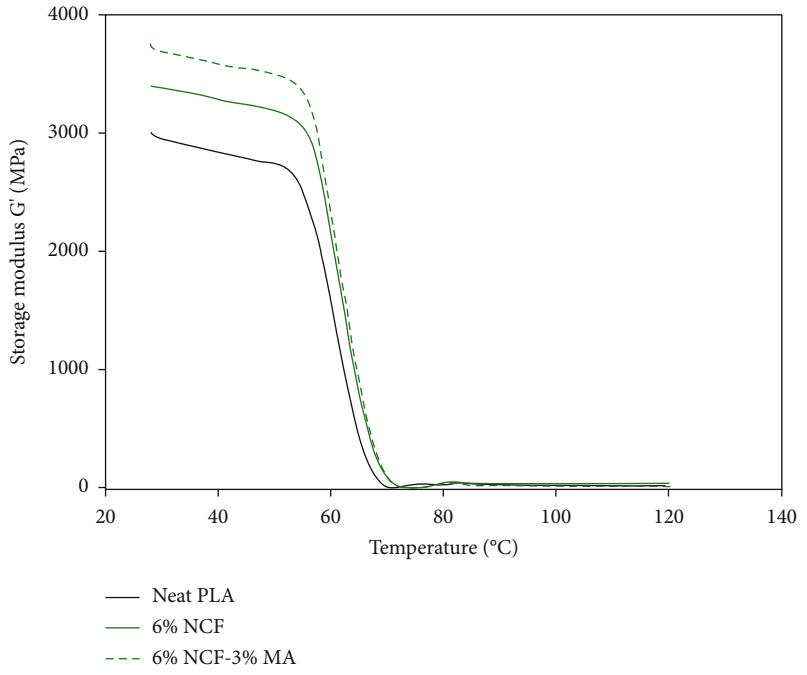

(b)

Figure 3: Continued.

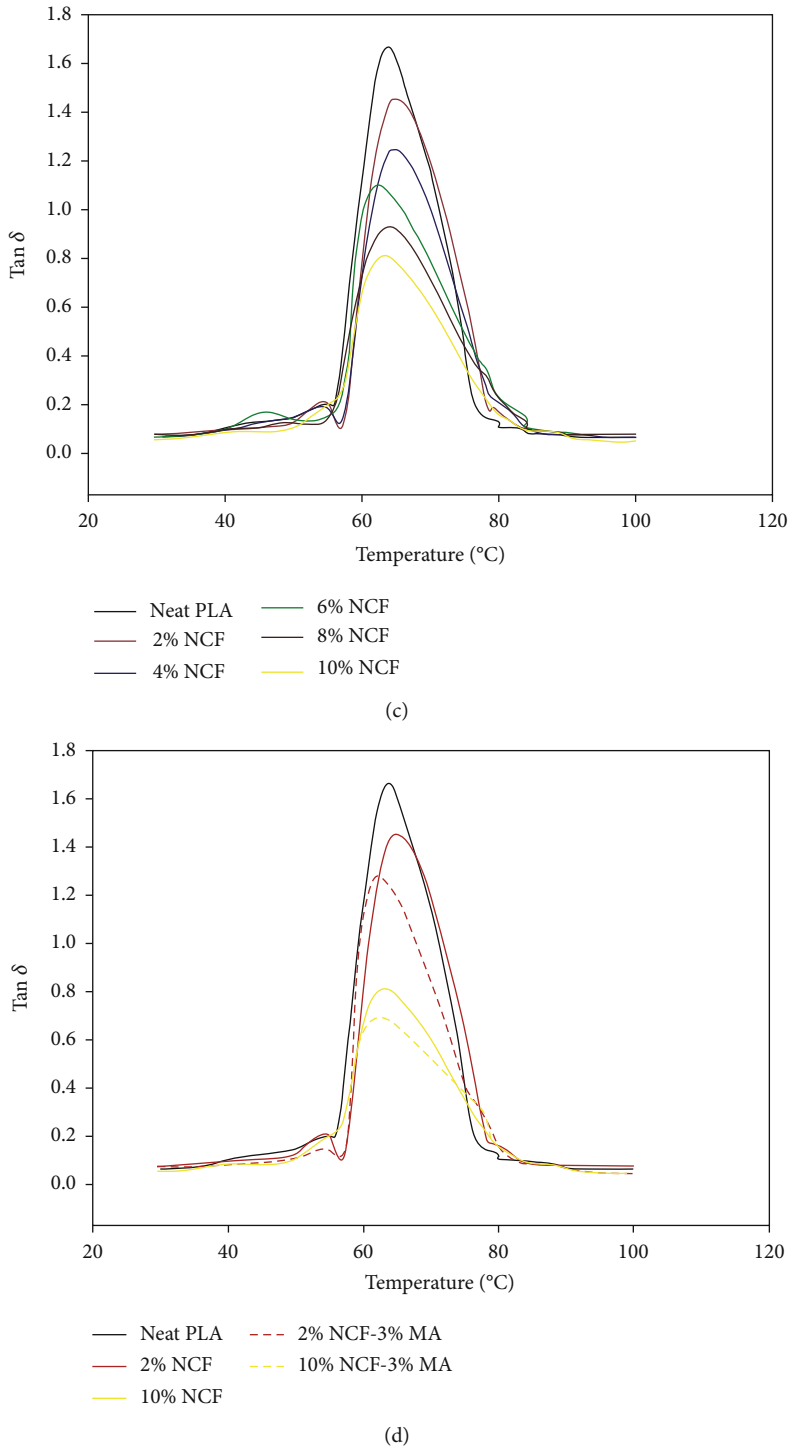

Figure 3: (a) Storage modulus G' of the PLA-NCF composite. (b) Storage modulus G' of PLA-6%NCF-3%MA. (c) tan δ of PLA-NCF. (d) tan δ of PLA-NCF-3%MA.

10% NCF in PLA. Meanwhile, the 3% addition of MA reduces the melting temperature up to 151.1°C of 10%NCF-PLA. Also, the glass transition temperature, T_g, reduces to 57.4°C from 59.4°C with the inclusion of MA and NCF in the PLA. The small reduction of melting and glass transition temperature may have taken place due to the reason that the NCF and MA do not form heterogeneous nucleation sites in the NCF-PLA composite. Also, Figure 1(b) and Table 1 illustrate that the crystallization temperature T_c of neat PLA changes to 123.5°C from 125.5°C when NCF and MA are added in the PLA matrix. The reduction in T_c demonstrates that NCF and MA restrict the mobility of PLA matrix chains for crystallization. The estimated PLA melting enthalpy ΔH_m is 24.9 J/g that reduces

Table 2: Mechanical properties of PLA-NCF-MA composites.

PLA/NCF/MA	Tensile strength (MPa)	Elastic modulus (GPa)	Elongation at break (%)	Impact strength (kJ/m^2)	Storage modulus (MPa)	tan δ
100/0/0	37.1 ± 0.90	0.87 ± 0.02	14.1 ± 0.28	5.32 ± 0.04	3025 ± 20	1.54 ± 0.01
98/2/0	38.9 ± 0.70	0.95 ± 0.03	13.9 ± 0.27	5.13 ± 0.06	3232 ± 19	1.45 ± 0.02
96/4/0	42.7 ± 0.68	1.01 ± 0.05	13.7 ± 0.31	4.86 ± 0.11	3350 ± 18	1.21 ± 0.01
94/6/0	43.6 ± 0.71	1.09 ± 0.03	13.4 ± 0.23	4.55 ± 0.10	3454 ± 15	1.11 ± 0.03
92/8/0	45.1 ± 0.59	1.17 ± 0.02	12.9 ± 0.18	4.29 ± 0.09	3642 ± 17	0.93 ± 0.01
90/10/0	47.6 ± 0.74	1.26 ± 0.01	12.5 ± 0.17	4.01 ± 0.08	3855 ± 16	0.81 ± 0.04
95/2/3	40.8 ± 0.61	1.08 ± 0.03	20.11 ± 0.31	5.64 ± 0.08	3410 ± 19	1.39 ± 0.02
93/4/3	47.9 ± 0.65	1.18 ± 0.02	19.7 ± 0.11	5.85 ± 0.07	3541 ± 15	1.14 ± 0.01
91/6/3	50.8 ± 0.64	1.29 ± 0.01	19.05 ± 0.22	5.90 ± 0.05	3734 ± 17	1.01 ± 0.03
89/8/3	52.1 ± 0.76	1.38 ± 0.06	18.4 ± 0.30	5.98 ± 0.08	3856 ± 18	0.71 ± 0.02
87/10/3	53.2 ± 0.69	1.45 ± 0.04	17.9 ± 0.11	6.21 ± 0.04	4060 ± 19	0.67 ± 0.01

to 20.7 J/g with the inclusion of 3% MA and 10% NCF. The peak width and height of cooling curves (Figure 1(b)) reduce with the introduction of 3% MA and NCF increments which decreases the melting enthalpy for PLA-NCF-FB composite.

Equation (1) was used to calculate the degree of crystallinity (X_c %) in PLA. Table 1 shows that the degree of crystallinity decreases from 14.9% to 9.8% when 10% NCF and 3% MA are added. The 37.4% decrease in X_c % demonstrates that the addition of NCF and MA did not initiate the nucleation site in PLA matrix. The FB and NCF obstruct the movement of PLA chains that result in the reduction of crystallization temperature (T_c). Furthermore, reduction in crystallinity accelerates the diffusivity and solubility of CO_2 in the polymer matrix [5]. The impermeability of crystalline zones hinders the diffusion of molecules due to close packed and regular chain structure that offers minimum free volume for solubility of CO_2. The reduction of crystallinity in PLA-NCF-MA composite indicates that the addition of NCF and MA increases the diffusivity and solubility of CO_2. The energy consumption during processing can be reduced by increased CO_2 solubility which also increases the diffusion coefficient acting as a potential plasticizer in the processes.

The contact angle of sessile drop of water is illustrated in Figure 2 for neat PLA and PLA-NCF-MA composite. The neat PLA has a contact angle of 78.9 ± 0.3°. The 10% NCF addition decreases the contact angle by 11 percent and reaches up to 70.7 ± .0.35° indicating the improvement in hydrophilic behaviour. Also, 3% MA inclusion in 10%NCF-PLA decreases the contact angle to 70.1 ± 0.35° demonstrating the minimum effect of MA on the composite wettability. The enhanced hydrophilic behaviour with inclusion of NCF shows the existence of hyroxyl groups increasing the wettability and hydrophilic behaviour in PLA-NCF. Also, the decrease in water contact angle with the inclusion of NCF increases the surface area providing the opportunity for distilled water to interact more with the surface of fiber. Additionally, the NCF decreases the surface roughness allowing adequate distribution of water leading to reduction of contact angle and enhancement in wetting of PLA-NCF-MA composite.

Figure 3 illustrates the loss factor (tan δ) and storage modulus (G') of composite with respect to temperature. Figure 3(a) illustrates that the storage modulus G' of PLA is 3010 MPa. In contrast to neat PLA, the storage modulus G' is increased up to 20% when 10% NCF is inserted in the PLA matrix. The storage modulus rises due to increased stiffness of the PLA matrix which is reinforced by NCF [35, 36]. Moreover, Figure 3(a) illustrates that the fall of NCF-PLA storage modulus occurs in the range of 56°C and 58°C due to glass transition temperature which is consistent with the results of DSC. The molecular mobility of the PLA matrix chain beyond the glass transition temperature can be the reason because storage modulus G' falls [36]. Figure 3(b), as an example, illustrates that the storage modulus of 6% NCF-PLA is 3454 ± 15 MPa which rises up to 3734 ± 17 MPa when 3% MA is added. The 10% increase in storage modulus with the addition of 3% MA in 6% NCF-PLA composite is due to enhancement in interfacial adhesion between the PLA matrix and NCF. Also, the interfacial adhesion might reduce the molecular mobility at the interfaces of NCF and PLA matrix. Table 2 demonstrates maximum storage modulus values showing enhancement in adhesion which might have occurred because of improvement in compatibility because of MA inclusion. The maleic anhydride (MA) compounds might have reacted to the hydroxyl groups in the NCF that consequently formed the ester bonds, and because of similar polarity, the PLA matrix intermingled with MA which acts as copolymer. The increase of storage modulus occurred due to improvement in interfacial adhesion after the addition of MA as interfacial modifier which linked the PLA matrix and NCF.

Figure 3(c) indicates that 1.55 is the mechanical damping tan δ for neat PLA. The increase of NCF in gradual increments of 10% reduces tan δ up to 0.81. The decrease in tan δ occurs because of restriction of PLA molecule movement instigated by stiff CNF [37]. Figure 3(d) illustrates the reduction in peak height of tan δ to 0.69 when 3% MA is

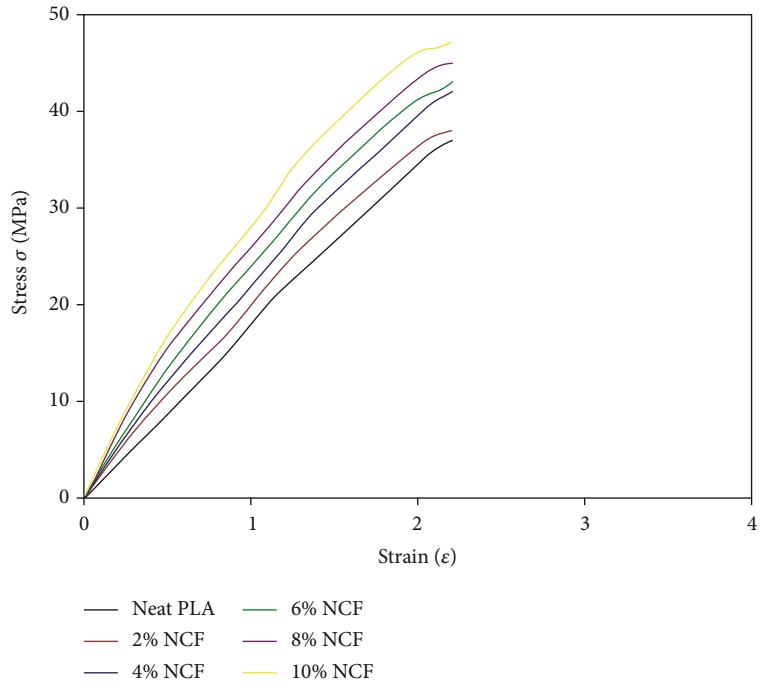

(a)

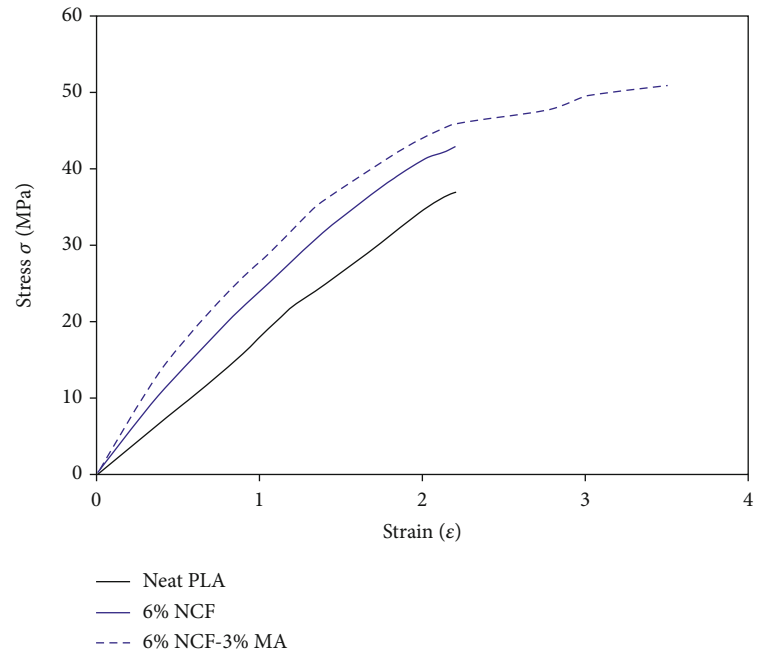

(b)

Figure 4: Continued.

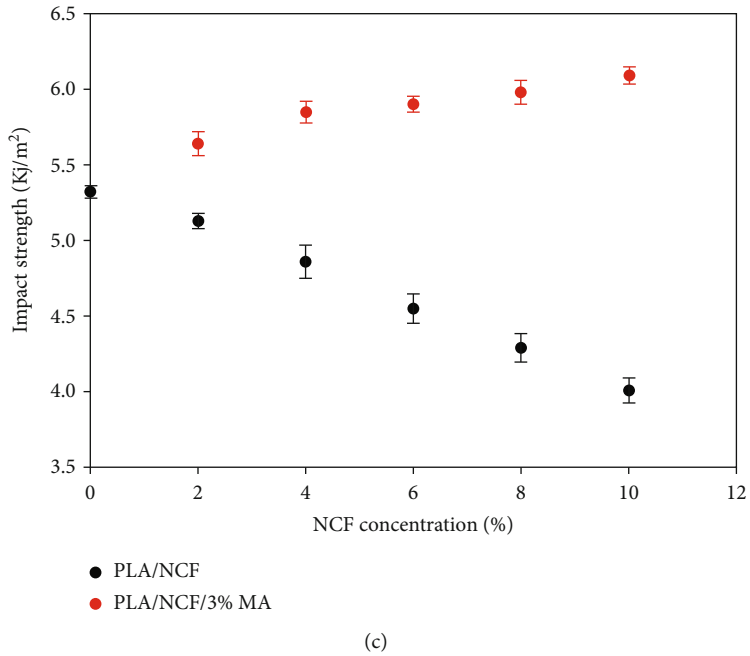

(c)

Figure 4: (a) Tensile curve of PLA-NCF. (b) Tensile curve of PLA-6%NCF-3%MA. (c) Impact strength of PLA-NCF-MA.

Table 3: Atomic % concentration, binding energy (BE), and bond type of C1s and O1s orbitals.

Bond type	Neat PLA		PLA-6% NCF		PLA-6%NCF-3%MA	
	BE (eV)	Atomic % concentration	BE (eV)	Atomic % concentration	BE (eV)	Atomic % concentration
O1s	532.33	22.74	532.31	26.93	532.29	34.59
C1s	284.83	77.01	284.79	72.89	284.95	65.25
O1s_1_O=C	532.09	12.61	532.07	13.82	532.05	14.81
O1s_2_O-C	533.42	10.15	533.33	13.19	533.38	19.70
C1s_1_C-C	284.79	54.65	248.68	47.95	248.85	33.39
C1s_2_C-O	286.38	13.36	286.32	15.35	286.34	18.26
C1s_3_O-C=O	288.90	8.98	288.82	9.67	288.85	13.69

added in 10%NCF-PLA signifying the advancement in interfacial adhesion. The results indicate that the reduction in tan δ increases molecular relaxation and aids the NCF-PLA composite to withstand greater amount of force. Finally, the impact of effective interfacial adhesion can be noticed in reduction of energy dissipation resulting in improved behaviour of energy absorption. Table 2 summarizes the tan δ values of PLA-NCF-MA composites.

Figures 4(a) and 4(b) demonstrate the tensile curves of PLA-NCF-MA composite. Table 2 shows the analogous data of % elongation at break, tensile strength, and elastic modulus. The tensile strength of neat PLA appears to be 37.1 ± 0.9 MPa, and it increases to 47.6 ± 0.74 MPa when the 10% NCF is added to the PLA matrix. Additionally, the insertion of 10% NCF in the PLA matrix increases the modulus of elasticity to 1.26 ± 0.01 MPa in comparison to neat PLA. The 10%NCF-PLA composite shows the improvement in elastic modulus up to 30.9% and tensile strength up to 22.1% when compared to neat PLA. The NCF content from 2% to 10% has negligible effect on the improvement of % elongation at break. The slight reduction in % elongation might have occurred due to the restriction of molecular mobility of PLA chains with the addition NCF. The noticeable increase in % elongation at break, tensile strength, and elastic modulus occurs with the addition of MA in the NCF-PLA composite. Figure 4(b) shows the addition of 3% MA in composite with 6% NCF-PLA increases tensile strength up to 26.9%, elastic modulus up to 32.5%, and % elongation at break up to 21.2% in comparison to neat PLA. The MA acted as interfacial compatibilizer which improved the interfacial adhesion and increased the mechanical properties of the NCF-PLA composite. In contrast to neat PLA, the 3% MA inclusion in 10%NCF-PLA demonstrates the increase of tensile strength up to 30.2%, % elongation at break up to 21.2%, and elastic modulus up to 40.0%. The improvement in mechanical properties might have happened due to the development of hydrogen bonds between the PLA matrix and NCF because of the presence of MA. The presence of strong hydrogen bonds also

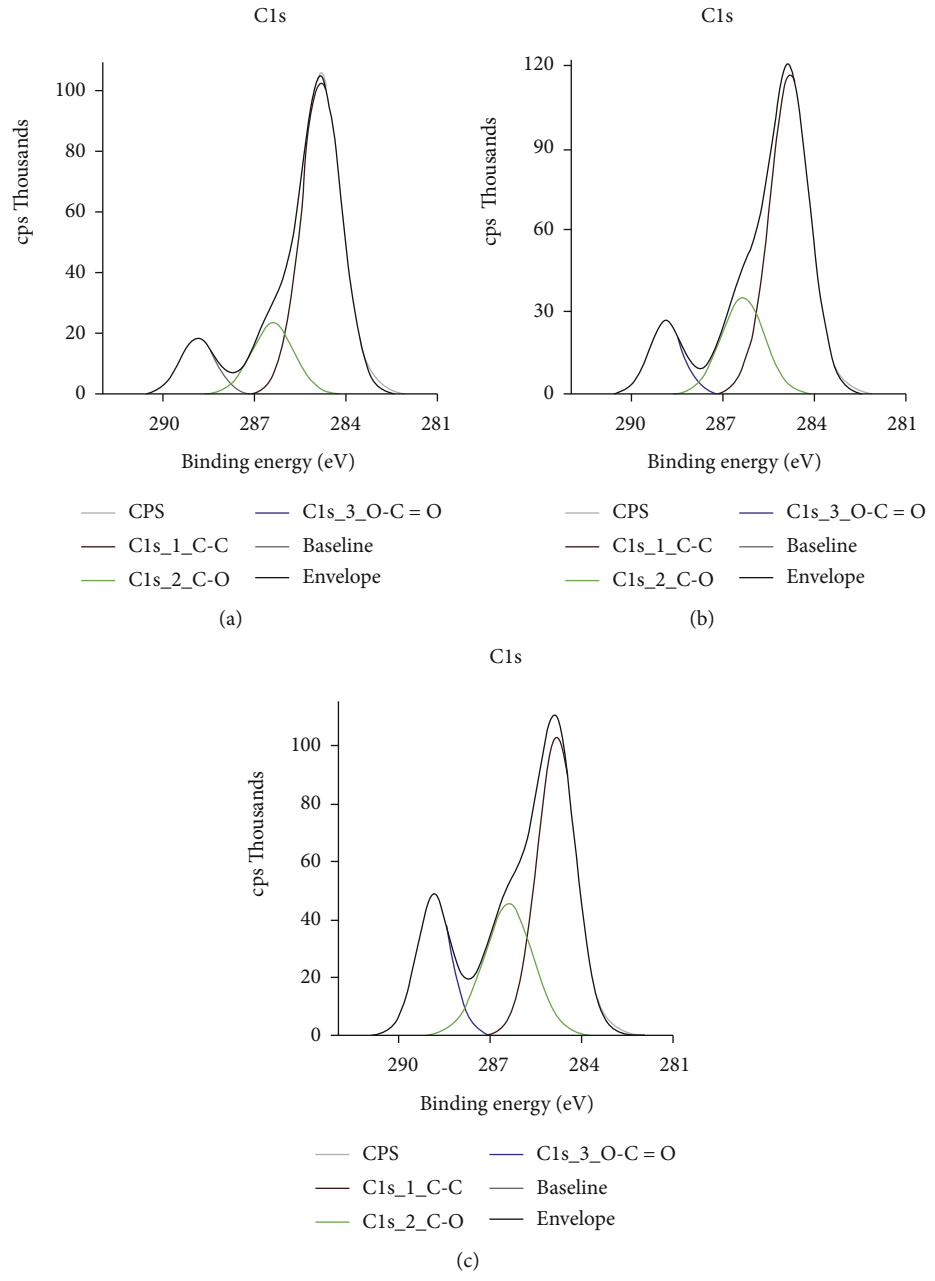

Figure 5: X-ray photo spectroscopy peaks in C1s and O1s orbitals: (a) neat PLA, (b) PLA-6%NCF composite, and (c) PLA-6%NCF-3%MA composite.

played a role in adequate dispersion of NCF in the PLA matrix resulting in capable load transfer from the PLA matrix to NCF [38].

Figure 4(c) indicates that incorporating NCF in PLA decreased impact strength up to 25% from 5.32 ± 0.04 kJ/m^2 to 4.01 ± 0.08 kJ/m^2 for the NCF-PLA composite. The addition of nanocellulose fibril decreases molecular mobility in the PLA matrix in turn reducing the energy absorption that decreases the impact strength of the NCF-PLA composite. Furthermore, the reduction of impact strength occurs because of inefficient stress transfer when nanocellulose fibril (NCF) is present as its presence obstructs the penetration of PLA between the nanofibrils. The enhancement in impact strength by the addition of 3% MA in 10%NCF-PLA can be noticed when compared to neat PLA as it is increases up to 15.3%. The MA as a coupling agent increased the interaction between NCF and PLA matrix resulting in strong interfacial adhesion and helped in effective load transfer. Also, the presence of MA causes the chain grafting between NCF and PLA matrix that increases the impact strength of composite due to effective energy absorption. The improvement in mechanical properties of the NCF-PLA composite is increased remarkably by the addition of MA which acts as interfacial modifier.

The carbon oxygen bond types were recognized by exposing the O1s and C1s regions of specimen by using

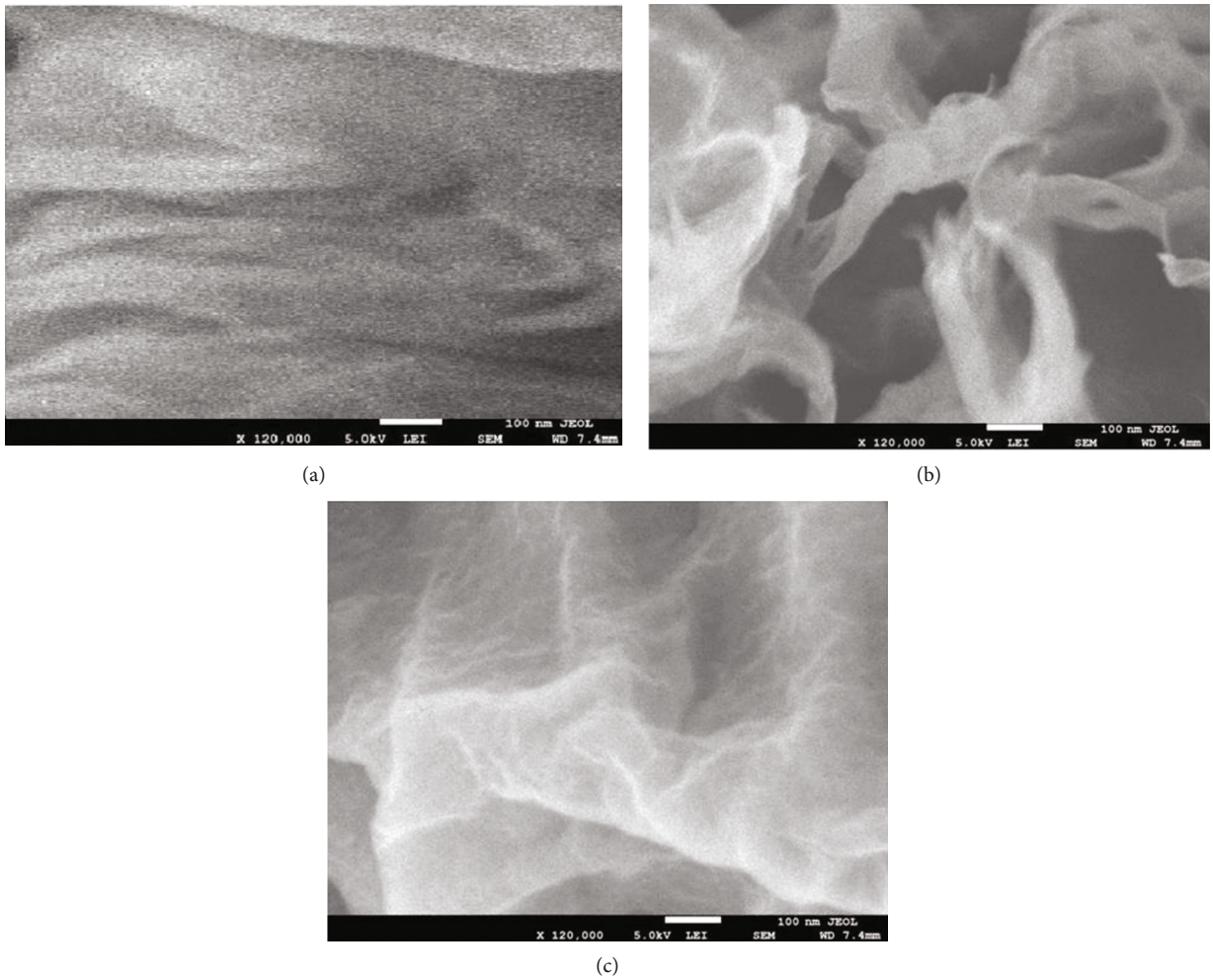

Figure 6: Fracture surface: (a) neat PLA, (b) PLA-6%NFC, and (c) PLA-6%NFC-3%MA.

XPS. Table 3 shows the bond type with their related energy of binding and atomic concentrations. Figure 5(a) demonstrates the peaks of pure PLA having corresponding intensities for functional groups related to the C1s region. The pure PLA polymer consists of covalent bond between oxygen, carbon, and hydrogen. In PLA matrix except hydrogen, 288.90 eV, 286.38 eV, 284.79 eV, 533.42 eV, and 532.09 eV binding energies are being presented for O–C=C bond, C–O bond, C–C bond, O=C bond, and O–C bond, respectively. Table 3 and Figure 5(b) illustrate that inclusion of 6% NCF in the PLA matrix elevates the carbon-oxygen bond concentration in the composite. The NCF contains higher level of carbon oxygen in its structure than PLA which increases the atomic % concentration of O-C=O to 9.67 atomic % from 8.98 atomic %. Moreover, in the PLA matrix, the atomic concentration of C-O bond increases to 15.35% from 13.36% due to the addition of NCF. In previous studies, it is shown that the corresponding binding energies of C-O bond and CC bond are 286.5 eV and 285.0 eV which correspond to our data [5]. The C-O, C-C, and C=O are the fundamental bonds of maleic anhydride (MA). The combinations of these bonds remarkably improve the grafting of carbon-oxygen bonds on the PLA matrix [38]. The presence of hydroxyl bonds in MA improves the properties of the NCF-PLA composite by increasing interaction between NCF and PLA. Figure 5(c) shows the increase in shoulder peak of the C1s region which might have occurred because of strong grafting creating better adhesion and crosslinking. The improvement can be attributed to the supplemented C-O bond concentration because of MA to 18.26 at.% from 13.36 at.% as shown in Table 3. Moreover, when compared to neat PLA, the O-C=O bond concentration increases to 13.69 at.% from 8.98 at.% as MA is added. Similar results were found with variable concentrations of NCF having 3% MA. The studies show that the MA might have shorter molecular chains than PLA making this as an attractive feature when it comes to effective creation of interfacial adhesion and crosslinking [39]. The effect is confirmed by analyzing the impact strength for the PLA-10%NCF-3%MA composite which improved 15% as shown in Table 2.

The tensile fracture surfaces of neat PLA, PLA-6%NCF, and PLA-6%NCF-3%MA are shown in Figure 6. Figure 6(a) shows smooth fracture arising from neat molecular attachment indicating the brittle nature of pure PLA. The addition of NCF in PLA demonstrated irregular surface pattern and voids in the cross section of fracture surface as shown in Figure 6(b) of PLA/6%NCF. The voids on fracture surface of PLA/6%NCF form because of pulling out of NCF

showing weak interfacial adhesion. Figure 6(c) shows the addition of 3% MA in PLA/6%NCF creates irregular fracture surface and decreases the voids as the reduction in debonding of NCF occurs due to increase in interfacial adhesion. The anhydride groups present in MA supplemented the adhesion by reacting with hydroxyl group on the NCF and PLA surfaces resulting in improvement of tensile and impact strength of the NCF-PLA-MA composite.

4. Conclusion

The study presents analysis of the PLA-NCF-MA composite developed by utilizing twin extruder. The addition of NCF in varying concentrations in PLA has shown minimum impact on degree of crystallinity in the NCF-PLA composite and does not act as nucleating agent. The presence of hydroxyl bonds in NCF increased hydrophilicity in the NCF-PLA composite. Furthermore, the molecular relaxation caused by MA increased the storage modulus and decreased tan δ. Also, the decrease in tan δ peak which resulted from molecular relaxation allows the PLA-NCF-MA composite to endure high energy of absorption. The addition of 3% MA increased the impact strength and % elongation at break illustrating the presence of strong interfacial adhesion between NCF and PLA. Moreover, the results show that interfacial adhesion increased due to the addition of MA which not only enhanced uniform dispersion of NCF but also reduced NCF pulling out from the PLA matrix.

Data Availability

All data are available within the manuscript.

Conflicts of Interest

The authors declare that they have no conflicts of interest.

Acknowledgments

The authors disclosed receipt of the following financial support for the research, authorship, and/or publication of this article. This project was funded by Deanship of Scientific Research (DSR) at King Abdulaziz University, Jeddah, under grant no. G1255-135-1440. The authors, therefore, acknowledge with thanks DSR for technical and financial support.

References

[1] E. Drumright, R. Gruber, and E. Henton, "Polylactic acid technology," *Advanced Materials*, vol. 12, no. 23, pp. 1841–1846, 2000.

[2] R. MacDonald, P. McCarthy, and A. Gross, "Enzymatic degradability of poly(lactide): effects of chain stereochemistry and material crystallinity," *Macromolecules*, vol. 29, no. 23, pp. 7356–7361, 1996.

[3] A. Mohanty, K. Misra, and G. Hinrichsen, "Biofibres, biodegradable polymers and biocomposites: An overview," *Macromolecules Materials Engineering*, vol. 276-277, no. 1, pp. 1–24, 2000.

[4] D. Feng, D. F. Caulfield, and A. R. Sanadi, "Effect of compatibilizer on the structure-property relationships of kenaf-fiber/polypropylene composites," *Polymer Composites*, vol. 22, no. 4, pp. 506–517, 2001.

[5] U. Saeed, M. Nawaz, and H. Al-Turaif, "Wood flour reinforced biodegradale PBS/PLA composite," *Journal of Composite Materials*, vol. 52, no. 19, pp. 2641–2645, 2018.

[6] A. Alemdar and M. Sain, "Biocomposites from wheat straw nanofibers: morphology, thermal and mechanical properties," *Composites Science and Technology*, vol. 68, no. 2, pp. 557–565, 2008.

[7] H. Yang, D. Gardner, and A. Nader, "Characteristic impact resistance model analysis of cellulose nanofibril-filled polypropylene composites," *Composites Part A Applied Science and Manufacturing*, vol. 42, pp. 2028–2034, 2011.

[8] J. Gardner, S. Oporto, and R. Mills, "Adhesion and surface issues in cellulose and nanocellulose," *Journal of Adhesion Science and Technology*, vol. 22, no. 5-6, pp. 545–567, 2008.

[9] P. Mathew, K. Oksman, and M. Sain, "Mechanical properties of biodegradable composites from poly lactic acid (PLA) and microcrystalline cellulose (MCC)," *Journal of Applied Polymer Science*, vol. 97, pp. 2014–2018, 2005.

[10] A. Ilyas, M. Sapuan, and L. Sanyang, "Nanocrystalline cellulose as reinforcement for polymeric matrix nanocomposites and its potential applications: a review," *Current Analytical Chemistry*, vol. 14, no. 3, pp. 203–208, 2018.

[11] A. Ilyas, M. Sapuan, and L. Sanyang, "Sugar palm nanofibrillated cellulose (Arenga pinnata (Wurmb.) Merr): effect of cycles on their yield, physic-chemical, morphological and thermal behaviour," *International Journal of Biological Macromolecules*, vol. 123, pp. 379–384, 2019.

[12] N. Bitinis, R. Verdejo, and P. Cassagnau, "Structure and properties of polylactide/natural rubber blends," *Materials Chemistry and Physics*, vol. 129, no. 3, pp. 823–831, 2011.

[13] P. Bordes, E. Pollet, and L. Ave'rous, "Nano-biocomposites: biodegradable polyester/nanoclay systems," *Progress in Polymer Science*, vol. 34, no. 2, pp. 125–155, 2009.

[14] A. Sorrentino, G. Gorrasi, and V. Vittoria, "Potential perspectives of bio-nanocomposites for food packaging applications," *Trends in Food Science and Technology*, vol. 18, pp. 84–95, 2007.

[15] A. L. Goffin, J. M. Raquez, and E. Duquesne, "From interfacial ring-opening polymerization to melt processing of cellulose nanowhisker-filled polylactide-based Nanocomposites," *Biomacromolecules*, vol. 12, no. 7, pp. 2456–2465, 2011.

[16] B. Dogu and C. Kaynak, "Behavior of polylactide/microcrystalline cellulose biocomposites: effects of filler content and interfacial compatibilization," *Cellulose*, vol. 23, pp. 611–622, 2016.

[17] A. Iwatake, M. Nogi, and H. Yano, "Cellulose nanofiber-reinforced polylactic acid," *Composites Science and Technology*, vol. 68, no. 9, pp. 2103–2106, 2008.

[18] K. Oksman, A. Mathew, and D. Bondeson, "Manufacturing process of cellulose whiskers/polylactic acid nanocomposites," *Composites Science and Technology*, vol. 66, no. 15, pp. 2776–2784, 2006.

[19] A. N. Frone, S. Berlioz, and J. F. Chailan, "Morphology and thermal properties of PLA-cellulose nanofibers composites," *Carbohydrate Polymers*, vol. 91, no. 1, pp. 377–384, 2013.

[20] M. Jonoobi, J. Harun, and P. Mathew, "Mechanical properties of cellulose nanofiber (CNF) reinforced polylactic acid (PLA)

prepared by twin screw extrusion," *Composites Science and Technology*, vol. 70, no. 12, pp. 1742–1747, 2010.

[21] S. Kalia, A. Dufresne, and B. M. Cherian, "Cellulose-based bio- and nanocomposites: a review," *International Journal of Polymer Science*, vol. 5, 35 pages, 2011.

[22] G. Siqueira, J. Bras, and A. Dufresne, "Cellulosic bionanocomposites: a review of preparation, properties and applications," *Polymers*, vol. 2, no. 4, pp. 728–765, 2010.

[23] H. A. Khalil, A. Bhat, and A. I. Yusra, "Green composites from sustainable cellulose nanofibrils: a review," *Carbohydrate Polymers*, vol. 87, no. 2, pp. 963–979, 2012.

[24] J. F. Zhang and X. Sun, "Mechanical properties of poly (lactic acid)/starch composites compatibilized by maleic anhydride," *Biomacromolecules*, vol. 5, pp. 1446–1451, 2004.

[25] A. C. Fowlks and R. Narayan, "The effect of maleated polylactic acid (PLA) as an interfacial modifier in PLA-talc composites," *Journal of Applied Polymer Science*, vol. 118, pp. 2810–2820, 2010.

[26] T. Yu, N. Jiang, and Y. Li, "Study on short ramie fiber/poly (lactic acid) composites compatibilized by maleic anhydride," *Composites Part A: Applied Science and Manufacturing*, vol. 64, pp. 139–146, 2014.

[27] D. Carlson, L. Nie, and R. Narayan, "Maleation of polylactide (PLA) by reactive extrusion," *Journal of Applied Polymer Science*, vol. 72, no. 4, pp. 477–485, 1999.

[28] L. Petersson and K. Oksman, "Biopolymer based nanocomposites: comparing layered silicates and microcrystalline cellulose as nanoreinforcement," *Composites Science and Technology*, vol. 66, no. 13, pp. 2187–2196, 2006.

[29] D. Plackett, "Maleated polylactide as an interfacial compatibilizer in biocomposites," *Journal of Polymers and the Environment*, vol. 12, pp. 131–138, 2004.

[30] A. K. Mohanty, M. Misra, and L. T. Drzal, "Surface modifications of natural fibers and performance of the resulting biocomposites: an overview," *Composite Interfaces*, vol. 8, no. 5, pp. 313–343, 2001.

[31] T. F. Salem, S. Tirkes, A. O. Akar, and U. Tayfun, "Enhancement of mechanical, thermal and water uptake performance of TPU/jute fiber green composites via chemical treatments on fiber surface," *E-Polymers*, vol. 20, pp. 133–143, 2020.

[32] K. Coskun, A. Mutlu, M. Dogan, and E. Bozaci, "Effect of various enzymatic treatments on the mechanical properties of coir fiber/poly (lactic acid) biocomposites," *Journal of Thermoplastic Composite Materials*, vol. 34, pp. 1066–1079, 2021.

[33] M. M. Kabir, H. Wang, K. T. Lau, and F. Cardona, "Chemical treatments on plant-based natural fibre reinforced polymer composites: an overview," *Composites Part B: Engineering*, vol. 43, no. 7, pp. 2883–2892, 2012.

[34] A. K. Bledzki and J. Gassan, "Composites reinforced with cellulose based fibres," *Progress in Polymer Science*, vol. 24, no. 2, pp. 221–274, 1999.

[35] L. A. Pothan, Z. Oommen, and S. Thomas, "Dynamic mechanical analysis of banana fiber reinforced polyester composites," *Composites Science and Technology*, vol. 63, pp. 283–292, 2003.

[36] N. Hameed, P. A. Sreekumar, and B. Francis, "Morphology, dynamic mechanical and thermal studies on poly(styrene-co-acrylonitrile) modified epoxy resin/glass fibre composites," *Composites Part A: Applied Science and Manufacturing*, vol. 38, no. 12, pp. 2422–2432, 2007.

[37] A. K. Rana, B. C. Mitra, and A. N. Banerjee, "Short jute fiber-reinforced polypropylene composites: dynamic mechanical study," *Journal of Applied Polymer Science*, vol. 71, no. 4, pp. 531–539, 1999.

[38] M. S. Nicole and M. Laurent, "Surface chemistry changes of weathered HDPE/wood-flour composites studied by XPS and FTIR spectroscopy," *Polymer Degradation and Stability*, vol. 1, pp. 1–9, 2004.

[39] J. Z. Lu, Q. Wu, and S. Harold, "Chemical coupling in wood fiber and polymer composites: a review of coupling agents and treatments," *Wood and Fiber Science*, vol. 32, pp. 88–99, 2000.